

Coordinate families for the Schwarzschild geometry based on radial timelike geodesics

Tehani K. Finch¹

¹NASA Goddard Space Flight Center
Greenbelt MD 20771

We explore the connections between various coordinate systems associated with observers moving inwardly along radial geodesics in the Schwarzschild geometry. Painlevé-Gullstrand (PG) time is adapted to freely falling observers dropped from rest from infinity; Lake-Martel-Poisson (LMP) time coordinates are adapted to observers who start at infinity with non-zero initial inward velocity; Gautreau-Hoffmann (GH) time coordinates are adapted to observers dropped from rest from a finite distance from the black hole horizon. We construct from these an LMP family and a proper-time family of time coordinates, the intersection of which is PG time. We demonstrate that these coordinate families are distinct, but related, one-parameter generalizations of PG time, and show linkage to Lemaitre coordinates as well.

I. INTRODUCTION

The Schwarzschild geometry is among the best known spacetimes of general relativity. Not only is it an exact analytic solution of the Einstein equations, it has significant physical relevance as an excellent approximation to the spacetime outside the sun, and therefore as the starting point for many experimental tests of general relativity [1]. The study of radial geodesics has long been a key tool for scrutinizing this spacetime, and coordinates adapted to null radial geodesics (ingoing and outgoing Eddington-Finkelstein (EF) coordinates) appear regularly in textbooks [1]-[3]. Coordinates adapted to *timelike* radial geodesics have received much less attention, however, and indeed rarely appeared in the literature before the 2000s.

Taylor and Wheeler in [4] categorize radial timelike geodesics in terms of objects that are said to be in “hail” frames, “drip” frames, and the “rain” frame. Objects in a hail frame have been hurled inward toward the black hole from an effectively infinite distance; they start at infinity with an initial inward velocity of magnitude v_∞ . Objects in a drip frame are dropped from rest, from a finite initial radius R_i . Between these two categories are objects in the rain frame, which can be thought of as having been dropped from rest, from infinitely far away. Objects in the rain frame represent the $R_i \rightarrow \infty$ limit of the set of drip frames and the $v_\infty \rightarrow 0$ limit of the set of hail frames. Apart from the treatments in [5] and [6], coordinates adapted to these frames have seldom been discussed as a group. This paper aims to provide a detailed clarification of the relationships between these sets of coordinates.

Meanwhile, the spatial volume contained within the event horizon of a black hole depends on the hypersurface of simultaneity used to compute it, and there are infinitely many possible values for this volume, each corresponding to a different time slicing. Calculations of black hole volume can prove useful for recognizing the attributes of various coordinate systems, as shown by DiNunno and Matzner in [7]. In a similar spirit, the present study utilizes volume calculations to as-

sist in the analysis of the coordinates affiliated with Schwarzschild radial timelike geodesics. These include the Lake-Martel-Poisson (LMP) coordinates of the hail frames, the Painlevé-Gullstrand (PG) and Lemaitre coordinates of the rain frame, and other coordinates, including those of Gautreau and Hoffmann (GH), of the drip frames ([5], [8]-[12]).

In this paper, we lay the groundwork with a discussion of PG time t_{PG} and its attributes in Section II. Then in section III we establish two separate extensions of PG time. The first is LMP time t_{LMP} , but the second is shown not to be GH time t_{GH} , but rather an offshoot of it we dub t_{DF} (drip frame proper time). In section IV we present t_{LMP^*} (the drip-frame analog of LMP time) and t_{HF} (hail frame proper time), which comprise the remaining pieces of a useful classification scheme. In this scheme, t_{LMP} , t_{PG} , and t_{LMP^*} correspond to the hail frame, rain frame, and drip frame variants, respectively, of an “LMP family” of time coordinates. Similarly, t_{HF} , t_{PG} , and t_{DF} correspond to hail frame, rain frame, and drip frame members of a “proper-time family” of time coordinates. The LMP and proper-time families represent two distinct generalizations of PG time.

The coordinate systems discussed in Sections II - IV make use of the familiar spherical coordinates $\{r, \theta, \phi\}$. The term “volume” will be used to refer to a spatial three-volume, meaning the proper volume of a region of a spacelike hypersurface. In the examples considered below (with the exception of static time), surfaces of constant time are spacelike everywhere, penetrate the horizon, and extend all the way to the singularity.

Henceforth units such that $G = c = 1$ will be adopted. Spacetime indices will be denoted by $\{a, b, c, \dots\}$. A coordinate ξ will be referred to as *timelike* if surfaces of constant ξ are spacelike hypersurfaces, and *spacelike* if surfaces of constant ξ are timelike hypersurfaces. Brackets $[]$ will be reserved for indicating the arguments of functions.

II. THE RAIN FRAME: PAINLEVÉ-GULLSTRAND COORDINATES

The familiar form of the Schwarzschild geometry with central mass m is given with respect to static coordinates $\{t_s, r, \theta, \phi\}$:

$$ds^2 = -\left(1 - \frac{2m}{r}\right) dt_s^2 + \frac{dr^2}{1 - 2m/r} + r^2 d\Omega^2. \quad (2.1)$$

It is useful to visualize the behavior of time coordinates

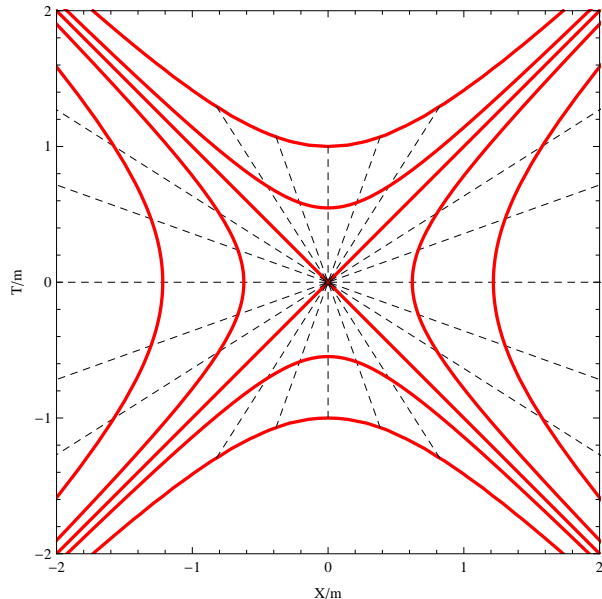


FIG. 1. Curves of constant t_s (dashed) and constant r (thick), for a Schwarzschild black hole. The line $T = X$ corresponds to the event horizon ($r = 2m, t_s = +\infty$) and the line $T = -X$ corresponds to the event horizon ($r = 2m, t_s = -\infty$). The uppermost hyperbolic curve represents the black hole/future singularity at $r = 0$ and the bottom hyperbolic curve is the white hole/past singularity, also at $r = 0$.

by means of a Kruskal diagram. In such a diagram, null trajectories have slopes of $\pm 45^\circ$, and the horizontal and vertical axes refer to the Kruskal-Szekeres coordinates X and T respectively. “Our universe” corresponds to the portion of the spacetime above and to the right of the line $T = -X$. The relation of Kruskal coordinates to static coordinates is discussed in, e.g., section 31.5 of [2]. Along with curves of constant r , curves of constant t_s are displayed in Figure 1. They do not penetrate the horizon, only approaching it asymptotically.

The Schwarzschild geometry expressed in Painlevé-Gullstrand [8, 9] coordinates $\{t_{PG}, r, \theta, \phi\}$ is given by

$$ds^2 = -\left(1 - \frac{2m}{r}\right) dt_{PG}^2 + 2\sqrt{\frac{2m}{r}} dt_{PG} dr + dr^2 + r^2 d\Omega^2; \quad (2.2)$$

we can immediately note the convenient property that the spatial PG three-metric is flat. This time coordinate

satisfies

$$dt_{PG} = dt_s + \frac{\sqrt{2m/r}}{1 - 2m/r} dr, \quad (2.3)$$

$$t_{PG} = t_s + 2\sqrt{2mr} - 2m \ln \left| \frac{\sqrt{r/2m} + 1}{\sqrt{r/2m} - 1} \right| + \mathcal{C}. \quad (2.4)$$

In (2.4) \mathcal{C} refers to an arbitrary constant of integration. The choice of $r = 0$ as the reference point will be adopted for all coordinates studied in this paper with the exception of Gautreau-Hoffmann time t_{GH} . The use of such a reference point implies that $\mathcal{C} = 0$, and thus

$$\lim_{r \rightarrow 0} t_{PG}[t_s, r] = t_s, \quad (2.5)$$

as seen in Figure 2. (We note that Hamilton and Lisle in [13] put forth a version of PG time that is defined with a reference point of $r = \infty$. Their version would require $\mathcal{C} = -\infty$ in (2.4), which would make t_{PG} take infinite negative values whenever both r and t_s are finite. Hence, we do not make use of it.)

The *normal observers* of a foliation are those whose four-velocities \vec{u} are orthogonal to the hypersurfaces of that foliation. Here, the normal observers of the PG slicing have been dropped from infinity and are thus in the rain frame. The observer’s velocity is radial and given by

$$\frac{dr}{d\tau} = -\sqrt{\frac{2m}{r}}. \quad (2.6)$$

She also has a conserved energy-at-infinity per unit rest mass, \tilde{E} , associated with the timelike Killing vector of the Schwarzschild geometry. For an observer in the rain frame $\tilde{E} = 1$. Intervals $\Delta\tau$ of proper time along an infalling $\tilde{E} = 1$ geodesic correspond precisely to intervals of t_{PG} [3, 4], so that $\Delta\tau = \Delta t_{PG}$. The four-velocity of such an observer is therefore given by

$$u^a := \frac{dx^a}{d\tau} = \left(1, -\sqrt{\frac{2m}{r}}, 0, 0\right). \quad (2.7)$$

We conclude this section by using PG coordinates to compute the black hole volume. Since the determinant of the three-metric, ${}^{(3)}g$, is $r^4 \sin^2 \theta$, the volume of a Schwarzschild black hole for the PG time slicing is simply

$$\begin{aligned} \text{Vol}_{PG} &= \int_0^{2\pi} \int_0^\pi \int_{r_{inner}}^{r_{outer}} \sqrt{{}^{(3)}g} dr d\theta d\phi \\ &= 4\pi \int_0^{2m} r^2 dr = \frac{4\pi}{3} (2m)^3 = \frac{32\pi}{3} m^3, \end{aligned} \quad (2.8)$$

which happens to coincide with the familiar volume for a sphere of radius $2m$ in Euclidean three-space. We will generalize (2.8) and provide hail-frame and drip-frame counterparts of many of these results in Sections III and IV.

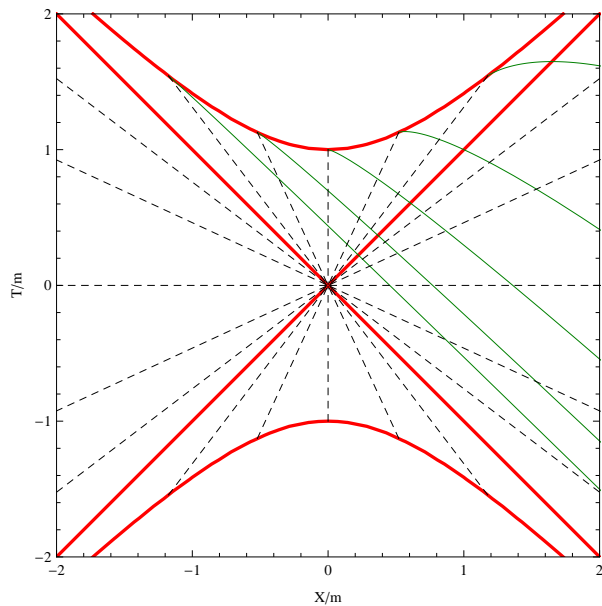


FIG. 2. Curves of constant t_{PG} (thin) superposed onto curves of constant t_s (dashed) and constant r (thick). From the left, the values shown are $t_{PG} = \{-4m, -2m, 0, 2m, 4m\}$ and they intersect the corresponding curves $t_s = \{-4m, -2m, 0, 2m, 4m\}$ at the (future) curve $r = 0$.

III. COORDINATES BASED ON GENERAL INGOING RADIAL GEODESICS

Having given a flavor for the attributes of PG time, we now consider coordinates based on a broader class of trajectories. The time coordinates discussed in this

section are adapted to radial timelike geodesics of the Schwarzschild geometry for particles with general values of \tilde{E} . A convenient choice of parameter is $p = 1/\tilde{E}^2$. The $p < 1$, $p = 1$ and $p > 1$ cases correspond to the hail frames, rain frame, and drip frames, respectively. If $p < 1$ one can associate p with an initial velocity via $v_\infty = \sqrt{1-p}$; if $p > 1$ one can associate p with an initial radius via $R_i = 2Mp/(p-1)$. The connections between these time coordinates (which were briefly treated in [6] and in the endnotes of [5]) will be used to group them into what we call the GH family, the LMP family, and the proper-time family.

A. The hail frames: Lake-Martel-Poisson coordinates

In [5] Martel and Poisson analyzed an extension of the PG coordinate system, previously discovered by Lake [11]. They considered geodesic observers with initial inward velocity of magnitude v_∞ ; these are the normal observers of the foliation and they have $\tilde{E} = 1/\sqrt{1-v_\infty^2} = 1/\sqrt{p}$, where $0 < p < 1$. The LMP time is not itself proper time of the normal observer with a given value of p ; rather, intervals of LMP time are proportional to intervals of proper time $\tau^{(p)}$ via $\Delta t_{LMP}^{(p)} = \sqrt{p} \Delta \tau^{(p)}$. The LMP time coordinates $\{t_{LMP}^{(p)}\}$ provide a straightforward extension of PG time to the $p < 1$ cases.

Explicitly, in LMP coordinates $\{t_{LMP}^{(p)}, r, \theta, \phi\}$, the four-velocities of these observers are given by

$$u^a = \left(\sqrt{p}, -\sqrt{\frac{1}{p} - \left(1 - \frac{2m}{r}\right)}, 0, 0 \right). \quad (3.1)$$

The LMP time coordinate satisfies¹

$$dt_{LMP}^{(p)} = dt_s + \frac{\sqrt{1-p(1-2m/r)}}{1-2m/r} dr, \quad (3.2)$$

$$t_{LMP}^{(p)} = t_s + 2m \left(\frac{r\sqrt{1-p(1-2m/r)}}{2m} + \ln \left| \frac{1 - \sqrt{1-p(1-2m/r)}}{1 + \sqrt{1-p(1-2m/r)}} \right| - \frac{1-p/2}{\sqrt{1-p}} \ln \left| \frac{\sqrt{1-p(1-2m/r)} - \sqrt{1-p}}{\sqrt{1-p(1-2m/r)} + \sqrt{1-p}} \right| \right), \quad (3.3)$$

and also (dropping the superscript)

$$\lim_{r \rightarrow 0} t_{LMP}[t_s, r] = t_s. \quad (3.4)$$

The Schwarzschild line interval in the LMP coordinates is given by

$$ds^2 = -(1-2m/r) dt_{LMP}^2 + p dr^2 + 2\sqrt{1-p(1-2m/r)} dt_{LMP} dr + r^2 d\Omega^2. \quad (3.5)$$

In contrast to (2.2), for $p \neq 1$ the spatial three-metric in (3.5) (and those for the rest of the coordinates in this section) is curved, as can be verified through a calculation

¹ The first term in parentheses of (3.3) corrects a slight error in the corresponding equation of [5] in which the square root was omitted.

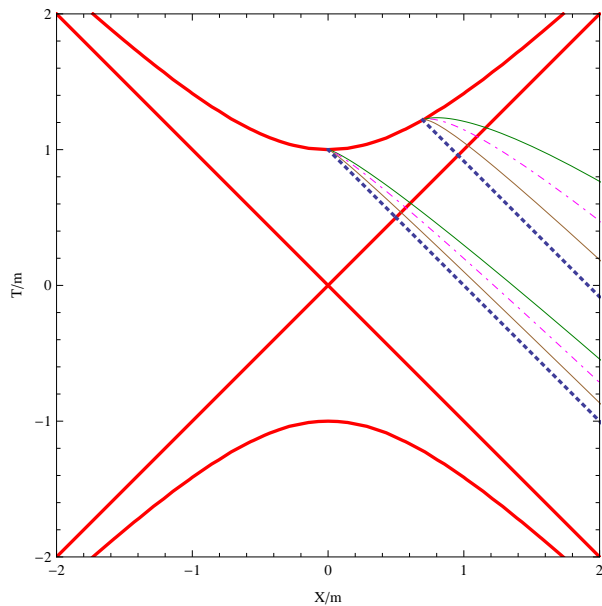


FIG. 3. Curves of constant t_{LMP} , shown along with thick dashed null curves of constant EF coordinate v , which is the $p \rightarrow 0$ limit of LMP time, for comparison. The curves within a bundle all meet at $r = 0$. The lower bundle corresponds to $t_{LMP} = 0$, the upper bundle to $t_{LMP} = 2.6m$. Within each bundle, from the bottom, the values of p are $\{0, 1/3, 2/3, 1\}$, where the $p = 1$ case is PG time.

of the three-dimensional Riemann tensor. It is useful to keep in mind that each value of p represents a different coordinate, and is thus associated with an entire foliation of the spacetime. Figure 3 shows that “bundles” of curves that correspond to a given value of t_{LMP} , but with different values of p , merge at $r = 0$. This is due to the fact that (3.4) holds regardless of p .

Turning our attention to the boundaries of the above range of p : in the limit $p \rightarrow 1$, we obtain PG time [5]. The limit $p \rightarrow 0$ results in the ingoing Eddington-Finkelstein (EF) coordinate v :

$$dv = dt_s + \frac{dr}{1 - 2m/r}, \quad (3.6)$$

$$v = t_s + r + 2m \ln \left| \frac{r}{2m} - 1 \right|, \quad (3.7)$$

$$ds^2 = -(1 - 2m/r) dv^2 + 2dv dr + r^2 d\Omega^2. \quad (3.8)$$

Slices of constant v are null; they follow the paths of ingoing radial light rays. This makes v itself a null coordinate. Thus, strictly speaking, v is not a time and is excluded from the LMP family introduced in Section IV A.

If $p < 1$, use of t_{LMP} specifies a different surface of simultaneity from that of t_{PG} , and the result for the vol-

ume inside a Schwarzschild black hole generalizes:

$$\text{Vol}_{LMP} = \int \sqrt{{}^{(3)}g} d^3x = 4\pi \int_0^{2m} \sqrt{p} r^2 dr = \frac{32\pi\sqrt{p}}{3} m^3. \quad (3.9)$$

This volume becomes arbitrarily small as $p \rightarrow 0$, *i.e.* as $v_\infty \rightarrow 1$.

B. The drip frames: Gautreau-Hoffmann coordinates

Coordinates inspired by the perspective of observers dropped from rest a finite distance from the black hole, *i.e.* in a drip frame, were introduced by Gautreau and Hoffmann in [12].² In this subsection we consider their coordinate system, which turns out not to relate to the PG coordinate system in the desired manner. Thus we will have to alter their time coordinate to arrive at a coordinate family that is a suitable outgrowth of PG time.

Freely falling observers dropped from rest at $r = R_i$ have a conserved energy-at-infinity per unit rest mass $\tilde{E} = \sqrt{1 - 2m/R_i}$. The proper time that elapses along their trajectories can be given in terms of r (the following is a slight modification of that given in Chapter 26 of [15] and is equivalent to that in Chapter 31 of [2]):

$$\tau^{(R_i)} = \frac{R_i^{3/2}}{(2m)^{1/2}} \left(\arccos \left[\sqrt{\frac{r}{R_i}} \right] + \sqrt{\frac{r}{R_i} - \left(\frac{r}{R_i} \right)^2} \right). \quad (3.10)$$

In this scheme, $\tau^{(R_i)} = 0$ corresponds to the instant at which the observer is dropped from $r = R_i$.

The quantity $\tau^{(R_i)}$, as given in (3.10), will not lead us to a suitable time coordinate; were we to attempt to use it, slices of constant $\tau^{(R_i)}$ would be slices of constant r and hence timelike hypersurfaces. Instead, the most useful form of $\tau^{(R_i)}$ is

$$\tau^{(R_i)} = \kappa t_s + h[r], \quad (3.11)$$

where κ is a constant and $h[r]$ is often called the “height function.” This is the type of transformation that keeps the metric stationary and the spherical symmetry manifest, as discussed in [6]. To obtain $\tau^{(R_i)}$ in this form, Gautreau and Hoffmann, rather than utilizing (3.10) directly, start with the geodesic equation. They arrive at the four-velocity for an observer in a drip frame in static coordinates $\{t_s, r, \theta, \phi\}$:

$$u^a = \left(\frac{\sqrt{1 - 2m/R_i}}{1 - 2m/r}, -\sqrt{\frac{2m}{r} - \frac{2m}{R_i}}, 0, 0 \right). \quad (3.12)$$

² The GH time coordinate should not be confused with that introduced by Novikov in [14], even though both are derived from $\tau^{(R_i)}$ of (3.10). The GH time coordinate is related to proper time readings of observers dropped from the *same* location at *different* times; vice versa for the Novikov time coordinate. Slices of constant Novikov time are in fact very different from those of constant GH time.

Equation (3.12) in turn gives

$$\frac{dt_s}{dr} = \frac{dt_s/d\tau^{(R_i)}}{dr/d\tau^{(R_i)}} = -\frac{\sqrt{1-2m/R_i}}{(1-2m/r)\sqrt{2m/r-2m/R_i}}, \quad (3.13)$$

and after some algebra, the combination of (3.12) and (3.13) yields

$$\frac{d\tau^{(R_i)}}{dr} = \sqrt{1-2m/R_i} \frac{dt_s}{dr} + \frac{\sqrt{2m/r-2m/R_i}}{1-2m/r}. \quad (3.14)$$

They then choose the initial location to be $\{t_s = 0, r = R_i\}$. This specifies a fiducial trajectory, and (3.14) now implies that the points *along this trajectory* satisfy

$$\tau^{(R_i)} = \sqrt{1-2m/R_i} \int_0^{t_s} d\tilde{t} + \int_{R_i}^r \frac{\sqrt{2m/\tilde{r}-2m/R_i}}{1-2m/\tilde{r}} d\tilde{r}. \quad (3.15)$$

The next step is to introduce a *general* coordinate

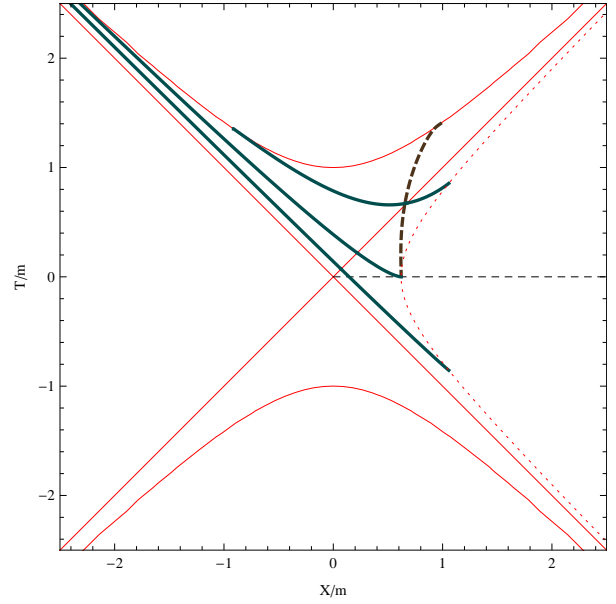


FIG. 4. Curves of constant $t_{GH}^{(R_i)}$ for a particular value of R_i . Here, $R_i = 2.25m$. The constant-time curves (thick solid) are for $t_{GH}^{(R_i)} = \{-1.5m, 0, 1.5m\}$. Also pictured is the trajectory (thick dashed) of an observer dropped from $r = R_i$ at $t_s = 0$. The hypersurface $t_s = 0$ (the portion of it outside the horizon, in our universe) is the thin dashed horizontal line, and the dotted hyperbola indicates $r = 2.25m$.

$t_{GH}^{(R_i)}$ that is allowed to take positive and negative values, and is valid for points both on and off the fiducial trajectory. This coordinate is defined such that the transformations between t_s and $t_{GH}^{(R_i)}$ take the same form as those for $\tau^{(R_i)}$ in (3.14) and (3.15):

$$dt_{GH}^{(R_i)} = \sqrt{1-2m/R_i} dt_s + \frac{\sqrt{2m/r-2m/R_i}}{1-2m/r} dr, \quad (3.16)$$

$$t_{GH}^{(R_i)} = \sqrt{1-2m/R_i} t_s + \sqrt{\frac{2m}{R_i}} \left(\sqrt{r(R_i-r)} + (R_i-4m) \left(\arctan \left[\sqrt{\frac{r}{R_i-r}} \right] - \frac{\pi}{2} \right) - \sqrt{2m(R_i-2m)} \ln \left| \frac{\sqrt{r(R_i-2m)} + \sqrt{2m(R_i-r)}}{\sqrt{r(R_i-2m)} - \sqrt{2m(R_i-r)}} \right| \right). \quad (3.17)$$

Here R_i is treated as a constant in (3.16) and (3.17), and both integrals in (3.15) have been evaluated explicitly. The Gautreau-Hoffmann time $t_{GH}^{(R_i)}$ is only defined for $r \leq R_i$, and furthermore it is assumed that $R_i > 2m$. Some curves of constant $t_{GH}^{(R_i)}$ are plotted along with the corresponding fiducial trajectory in Figure 4 for the case of $R_i = 2.25m$. The line interval has the form (drop-

ping the superscript)

$$ds^2 = -\frac{1}{1-2m/R_i} (1-2m/r) dt_{GH}^2 + \frac{2\sqrt{2m/r-2m/R_i}}{1-2m/R_i} dt_{GH} dr + \frac{dr^2}{1-2m/R_i} + r^2 d\Omega^2. \quad (3.18)$$

Unlike the other coordinates that have been discussed, $t_{GH}^{(R_i)}$ is defined with respect to a reference point of

$r = R_i$ (as opposed to $r = 0$) in the sense that

$$\lim_{r \rightarrow R_i} t_{GH}^{(R_i)}[t_s = 0, r] = 0. \quad (3.19)$$

Equation (3.19) is consistent with the fact that the hypersurface $t_{GH}^{(R_i)} = 0$ starts on the line $t_s = 0$ for any $R_i > 2m$; a few examples are shown graphically in Figure 5. However, this implies that when we consider the

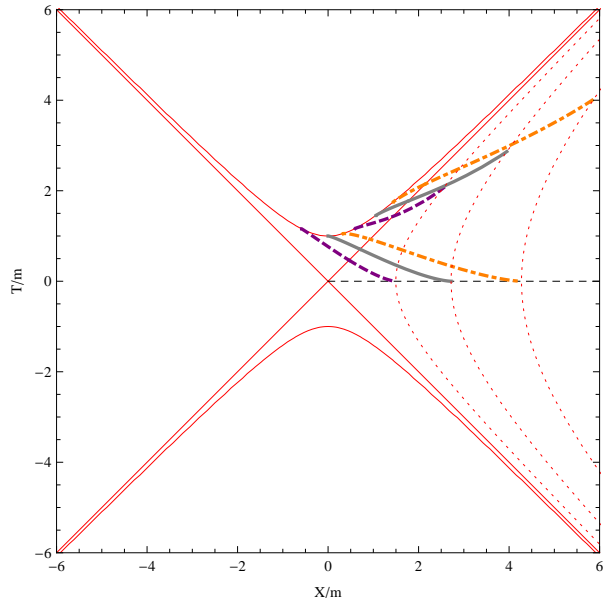


FIG. 5. Curves of constant $t_{GH}^{(R_i)}$ for various values of R_i . The lower bundle corresponds to $t_{GH}^{(R_i)} = 0$, the upper to $t_{GH}^{(R_i)} = 2.6m$. Within each bundle, the values of p are 3 (thick dashed), 2 (thick solid), and $5/3$ (thick dot-dashed); these curves correspond to $R_i = 3m, 4m$, and $5m$ respectively. (The $p = 1$ case is not well defined for this coordinate.) The hypersurface $t_s = 0$ (the portion of it outside the horizon, in our universe) is the thin dashed horizontal line on which the curves of the lower bundle begin, at $r = R_i$. Plots of $r = 3m, 4m$, and $5m$ (the dotted hyperbolae) are included for clarity.

$r \rightarrow 0$ limit of $t_{GH}^{(R_i)}$, a slight complication arises:

$$\lim_{r \rightarrow 0} t_{GH}^{(R_i)}[t_s = 0, r] = \pi(4m - R_i) \sqrt{\frac{m}{2R_i}} \neq 0, \quad (3.20)$$

in contrast to the behavior of t_{PG} in (2.5) and t_{LMP} in (3.4). Equation (3.20) implies that the $R_i \rightarrow \infty$ limit of $t_{GH}^{(R_i)}$ does not have a well-defined correspondence with PG time (this would be no different had we chosen any other finite value of \mathcal{C} in (2.4)); this limit differs from PG time by an infinite constant.³ Therefore, t_{GH} is *not* the $p > 1$ analog of t_{PG} that we seek.

³ Another way of stating this is that the difficulty with the $R_i \rightarrow \infty$ limit of $t_{GH}^{(R_i)}$ is due to the infinite transit time from $r = \infty$ to

To construct a coordinate that possesses the desired correspondence with PG time, and can easily be compared to LMP time, we keep (3.20) in mind and introduce

$$t_{DF}^{(R_i)} := t_{GH}^{(R_i)} - \pi(4m - R_i) \sqrt{\frac{m}{2R_i}}. \quad (3.21)$$

As was the case with $t_{GH}^{(R_i)}$, surfaces of constant $t_{DF}^{(R_i)}$ cannot be extended outward past $r = R_i$. Since these geodesics are those of observers in drip frames, we will refer to $t_{DF}^{(R_i)}$ as “drip-frame proper time” (or DF time).

The advantage of using R_i is that the allowed range of the r coordinate is clear. However, to facilitate comparison between coordinates, and the formulation of coordinate families, we will present our expressions in terms of p . We recall that if $p > 1$,

$$R_i = 2m p / (p - 1) \leftrightarrow p = \frac{R_i}{R_i - 2m}. \quad (3.22)$$

The range $\infty > R_i > 2m$, corresponds to $1 < p < \infty$. Combining (3.21) with (3.22) tells us that

$$t_{DF}^{(p)} = t_{GH}^{(p)} - \frac{\pi m (p - 2)}{\sqrt{p(p - 1)}}. \quad (3.23)$$

Naturally, since $t_{DF}^{(p)}$ and $t_{GH}^{(p)}$ differ only by an additive constant, intervals of $t_{DF}^{(p)}$ still have a correspondence with the proper time of an observer dropped from $r = R_i$, in that $\Delta t_{DF}^{(p)} = \Delta \tau^{(p)}$ between two given events.

The *GH family* of time coordinates we define to include the set $\{t_{GH}^{(p)}\}$; the set of time coordinates $\{t_{DF}^{(p)}\}$ will later be incorporated into the *proper-time family*.⁴ Notable from (3.21) is the fact that $t_{DF}^{(p)}$ reduces to $t_{GH}^{(p)}$ for the case $R_i = 4m$, which corresponds to $p = 2$. A comparison of Figure 5 to Figure 6 helps illustrate that the $\{t_{DF}^{(p)}\}$ as a set has a nontrivial difference from the set $\{t_{GH}^{(p)}\}$. One example of this is that these two figures have opposite “ordering” of the $p = 5/3$, $p = 2$ and $p = 3$ curves within the bundles.

In DF coordinates, the four-velocity of radial geodesic observers can be written as

$$\begin{aligned} u^a &= \left(1, -\sqrt{\frac{2m}{r} - \frac{2m}{R_i}}, 0, 0 \right) \\ &= \left(1, -\sqrt{\frac{1}{p} - \left(1 - \frac{2m}{r}\right)}, 0, 0 \right). \end{aligned} \quad (3.24)$$

finite values of r . Reference [12] points this out, although without explicitly mentioning PG time. Now, this particular difficulty could be avoided if one were to start with the Hamilton-Lisle version of PG time from [13], but we choose not to do so for reasons given in Section II.

⁴ Although in this paper the designations “drip-frame time” and “proper-time family” are associated only with $t_{DF}^{(p)}$, it should be emphasized that physically, *both* $\Delta t_{GH}^{(p)}$ and $\Delta t_{DF}^{(p)}$ correspond to proper time intervals of an observer in a drip frame.

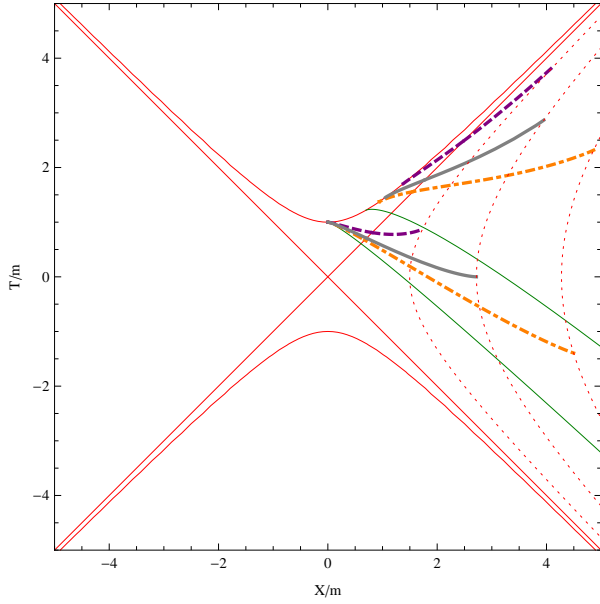


FIG. 6. Curves of constant t_{DF} . Unlike Figure 3, here the curves of the upper bundle do not meet at $r = 0$. The lower bundle corresponds to $t_{DF} = 0$, the upper to $t_{DF} = 2.6m$. Within each bundle, from the bottom, the values of p are $\{1, 5/3, 2, 3\}$. Plots of $r = 3m, 4m$, and $5m$ (the dotted hyperbolae) are included for clarity. The $p = 1$ case is PG time.

The coordinate transformations for $t_{DF}^{(p)}$ are (dropping the superscript)

$$dt_{DF} = \frac{dt_s}{\sqrt{p}} + \frac{1}{\sqrt{p}} \frac{\sqrt{1-p(1-2m/r)}}{1-2m/r} dr, \quad (3.25)$$

$$t_{DF} = \frac{1}{\sqrt{p}} \left(t_s + r \sqrt{1-p(1-2m/r)} - \frac{2m(p-2)}{\sqrt{p-1}} \arctan \left[\sqrt{\frac{p-1}{1-p(1-2m/r)}} \right] - 2m \ln \left| \frac{1 + \sqrt{1-p(1-2m/r)}}{1 - \sqrt{1-p(1-2m/r)}} \right| \right). \quad (3.26)$$

The expression for the metric⁵ becomes

$$ds^2 = -p(1-2m/r) dt_{DF}^2 + p dr^2 + 2\sqrt{p}\sqrt{1-p(1-2m/r)} dt_{DF} dr + r^2 d\Omega^2. \quad (3.27)$$

Like t_{PG} and t_{LMP} , t_{DF} is defined relative to $r = 0$, and the $p \rightarrow 1$ limit of t_{DF} is in fact PG time.

Comparing (3.25) with (3.2) shows that dt_{DF} and dt_{LMP} have a similar form, but the factor of $1/\sqrt{p}$ that

distinguishes them has nontrivial consequences: equation (3.26) implies that

$$\lim_{r \rightarrow 0} t_{DF}^{(p)}[t_s, r] = \frac{t_s}{\sqrt{p}}, \quad (3.28)$$

in contrast to (3.4). The fact that the right-hand side of (3.28) depends on p implies that curves of constant t_{DF} within the same bundle will not in general converge to the same $\{X, T\}$ point on the $r = 0$ surface, contrary to what occurs in bundles of t_{LMP} (this can be seen by comparing the upper bundles of Figure 3 and Figure 6). The spatial volume of the black hole for a slice of constant t_{DF} has the same form as that in (3.9):

$$\text{Vol}_{DF} = \int \sqrt{{}^{(3)}g} d^3x = 4\pi \int_0^{2m} \sqrt{p} r^2 dr = \frac{32\pi\sqrt{p}}{3} m^3. \quad (3.29)$$

This volume becomes arbitrarily large as p approaches ∞ , *i.e.* as $R_i \rightarrow 2m$.

For completeness we note that since, for any p , $dt_{GH}^{(p)} = dt_{DF}^{(p)}$, the metric written in terms of p for GH coordinates has the same form as (3.27), and the black hole volume for a slice of constant t_{GH} is also the same:

$$ds^2 = -p(1-2m/r) dt_{GH}^2 + 2\sqrt{p}\sqrt{1-p(1-2m/r)} dt_{GH} dr + p dr^2 + r^2 d\Omega^2, \quad (3.30)$$

$$\text{Vol}_{GH} = 4\pi \int_0^{2m} \sqrt{p} r^2 dr = 32\pi\sqrt{p} m^3/3. \quad (3.31)$$

IV. COMPLETING THE LMP AND PROPER-TIME FAMILIES

A. A $p > 1$ analog of t_{LMP}

The next step in constructing our coordinate families is obtaining a drip-frame analog of the set of LMP times. As with $t_{DF}^{(p)}$, these coordinates cannot be extended past $r = 2mp/(p-1)$, and they can be expressed in terms of R_i but not v_∞ . The $p > 1$ version of LMP time we denote as $t_{LMP*}^{(p)}$. The infinitesimal coordinate transformation between dt_s and dt_{LMP*} is the same as in (3.2), but, since $p > 1$, the finite coordinate transformation differs from (3.3):

$$dt_{LMP*}^{(p)} = dt_s + \frac{\sqrt{1-p(1-2m/r)}}{1-2m/r} dr, \quad (4.1)$$

$$t_{LMP*}^{(p)} = t_s + r \sqrt{1-p(1-2m/r)} - \frac{2m(p-2)}{\sqrt{p-1}} \arctan \left[\sqrt{\frac{p-1}{1-p(1-2m/r)}} \right] - 2m \ln \left| \frac{1 + \sqrt{1-p(1-2m/r)}}{1 - \sqrt{1-p(1-2m/r)}} \right|. \quad (4.2)$$

In fact, comparison with (3.26) shows that formally

⁵ Although they do not give it in explicit form, the authors of [16] show that it is possible to arrive at the metric of (3.27), as well as the PG metric (2.2), through analysis of the action for geodesics in Schwarzschild spacetime.

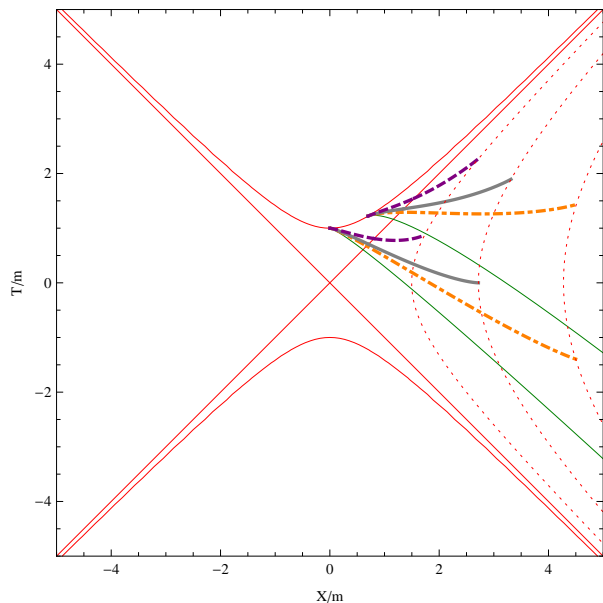


FIG. 7. Curves of constant t_{LMP*} . The lower bundle corresponds to $t_{LMP*} = 0$, the upper bundle to $t_{LMP*} = 2.6m$. Within each bundle, from the bottom, the values of p are $\{1, 5/3, 2, 3\}$, where the $p = 1$ case is PG time. Plots of $r = 3m, 4m$, and $5m$ (the dotted hyperbolae) are included for clarity.

$$t_{LMP*}^{(p)} = \sqrt{p} t_{DF}^{(p)}. \quad (4.3)$$

Thus, for any p , a slice of constant $t_{LMP*}^{(p)}$ is a slice of constant $t_{DF}^{(p)}$ and vice versa. Equation (4.3) indicates that for a *given* value of p , the coordinate $t_{LMP*}^{(p)}$ differs from the corresponding $t_{DF}^{(p)}$ only by an overall factor. Yet *as a collective*, the set $\{t_{LMP*}^{(p)}\}$ differs from $\{t_{DF}^{(p)}\}$ nontrivially. For example, curves of constant $t_{LMP*}^{(p)}$ within the same bundle converge at $r = 0$ (just as occurs with $t_{LMP}^{(p)}$) while those of constant $t_{DF}^{(p)}$ in general do not. This contrast becomes evident in a comparison of the upper bundle of Figure 6 with that of Figure 7.

The metric with respect to t_{LMP*} is given by

$$ds^2 = -(1 - 2m/r) dt_{LMP*}^2 + 2\sqrt{1 - p(1 - 2m/r)} dt_{LMP*} dr + p dr^2 + r^2 d\Omega^2, \quad (4.4)$$

the same form as (3.5). The normal observers have a four-velocity identical to that in (3.1). The evaluation of the black hole volume along slices of constant t_{LMP*} gives

$$\text{Vol}_{LMP*} = 4\pi \int_0^{2m} \sqrt{p} r^2 dr = \frac{32\pi\sqrt{p}}{3} m^3. \quad (4.5)$$

Curves of constant t_{LMP*} are shown by themselves in Figure 7 and together with curves of constant t_{LMP} in the top panel of Figure 9. Establishing t_{LMP*} as the $p > 1$

analog of t_{LMP} allows us to see $t_{LMP}^{(p)}$, t_{PG} , and $t_{LMP*}^{(p)}$ as encompassing, respectively, the $0 < p < 1$, $p = 1$, and $1 < p < \infty$ constituents of a one-parameter family of coordinates, which we call the *LMP family*. Appendix B discusses how the time coordinates in this family are related to the four-velocities of normal observers via

$$u_a = -\frac{1}{\sqrt{p}} \partial_a t. \quad (4.6)$$

B. A $p < 1$ analog of t_{DF}

Finally, we provide a hail-frame analog of t_{DF} . Recall that the distinguishing feature of DF time is that $\Delta t_{DF}^{(p)} = \Delta \tau^{(p)}$ for an observer with $p > 1$. The desired analog $t_{HF}^{(p)}$ (with “HF” indicating “hail frame”) would have $\Delta t_{HF}^{(p)} = \Delta \tau^{(p)}$ for an observer moving along an inward geodesic with $p < 1$, and would generalize a key property of the PG coordinate system. Such a

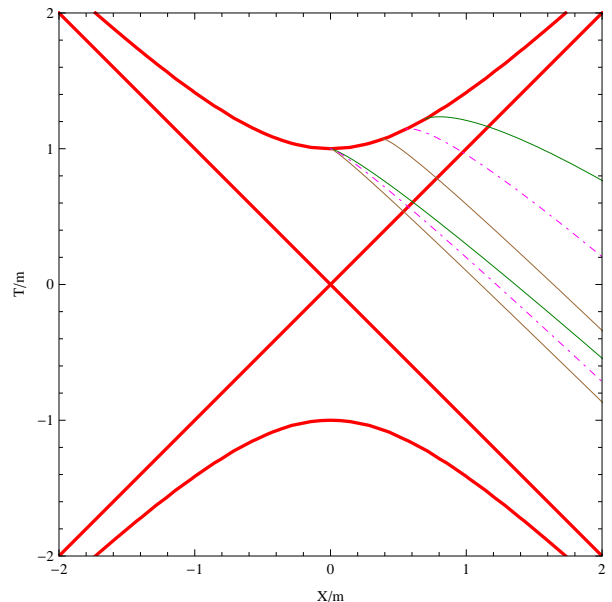


FIG. 8. Curves of constant t_{HF} . The lower bundle corresponds to $t_{HF} = 0$, the upper bundle to $t_{HF} = 2.6m$. Within each bundle, from the bottom, the values of p are $\{1/3, 2/3, 1\}$, where the $p = 1$ case is again PG time.

coordinate $t_{HF}^{(p)}$ is given by

$$t_{HF}^{(p)} = \frac{t_{LMP}^{(p)}}{\sqrt{p}}, \quad (4.7)$$

where $t_{LMP}^{(p)}$ is given in (3.3), and satisfies

$$dt_{HF}^{(p)} = \frac{dt_s}{\sqrt{p}} + \frac{1}{\sqrt{p}} \frac{\sqrt{1 - p(1 - 2m/r)}}{1 - 2m/r} dr, \quad (4.8)$$

the same form as (3.25). As noted in Section III A, the

$p \rightarrow 0$ limit of t_{HF} is not well defined. This is because the $p \rightarrow 0$ limit is associated with null trajectories, and proper time is not defined on a null trajectory. Curves of constant t_{HF} are plotted by themselves in Figure 8 and together with curves of constant t_{DF} in the bottom panel of Figure 9.

The resulting metric is given by

$$ds^2 = -p(1 - 2m/r) dt_{HF}^2 + 2\sqrt{p}\sqrt{1 - p(1 - 2m/r)} dt_{HF} dr + p dr^2 + r^2 d\Omega^2, \quad (4.9)$$

and the four-velocity of the normal observers is identical to that in (3.24). The volume computation reproduces the familiar result

$$\text{Vol}_{HF} = 4\pi \int_0^{2m} \sqrt{p} r^2 dr = \frac{32\pi\sqrt{p}}{3} m^3. \quad (4.10)$$

The time intervals $\Delta t_{HF}^{(p)}$, Δt_{PG} , and $\Delta t_{DF}^{(p)}$ all coincide with the proper time intervals of their respective normal observers; thus $t_{HF}^{(p)}$, t_{PG} , and $t_{DF}^{(p)}$ correspond to the $0 < p < 1$, $p = 1$, and $1 < p < \infty$ members of a *proper-time family*. They are all defined with respect to a reference point of $r = 0$, and they all satisfy

$$u_a = -\partial_a t, \quad (4.11)$$

on which we elaborate in Appendix B. Thus the proper-time family constitutes perhaps the most direct generalization of PG coordinates.

Despite their simplicity, the fact that the relations (4.3) and (4.7) depend on p has significant consequences. These include the contrast between the top and bottom panels of Figure 9; for the LMP family the curves within a bundle do not cross each other and converge to a point at $r = 0$. In the case of the proper-time family, the curves within a bundle do cross if the bundle corresponds to a negative value of the time coordinates, and generally do not meet at $r = 0$ (the exception being the $t = 0$ bundle). There is also the fact that the LMP family has a well-defined $p \rightarrow 0$ limit, but the proper-time family does not. Furthermore, only for the LMP family do the g_{tt} components of the metrics enjoy the same form, namely $-(1 - 2m/r)$, that is familiar from static coordinates. It is thus seen that although the LMP and proper-time families are related, there are still disparities between them.

V. DISCUSSION

It is now well understood that, due to general covariance, the predictions of general relativity for behavior of a physical system are independent of the coordinates used to describe them. Nonetheless, the choice of coordinates can be very significant, because this choice often has much influence on both the manageability of the calculations and on the amount of physical insight gained from them. Examples in which PG coordinates have proven useful include the “river model” of Schwarzschild

spacetime in which space itself flows inward toward the horizon, through a flat background [13]; the description of Hawking radiation as a tunneling process [17]; and analytic models of gravitational collapse [18]. Meanwhile, GH coordinates have been exploited for comparing massive particle trajectories in black hole and wormhole spacetimes [19]; in addition they have inspired the discovery of GH-type coordinates for de Sitter spacetime [20], which have been utilized in the description of a Schwarzschild mass [21] (and more recently a Reissner-Nordström charged mass [22]), embedded in a cosmological background.

With those developments as a backdrop, the present exposition has examined time coordinates adapted to general ingoing timelike radial geodesics in the Schwarzschild geometry. To obtain proper-time analogs of PG time for the drip frames and hail frames, we have introduced the coordinates $t_{DF}^{(p)}$ and $t_{HF}^{(p)}$, respectively; to our knowledge, analysis of these coordinates has not occurred elsewhere. We have also provided a drip-frame analog of LMP time in $t_{LMP*}^{(p)}$. The fact that the result $\frac{32\pi}{3}\sqrt{p}m^3$ for the Schwarzschild black hole volume is valid for all of the coordinate systems studied exhibits the close relation between them.

We have chosen to group these coordinates into a GH family $\{t_{GH}^{(p)}\}$, an LMP family $\{t_{LMP}^{(p)}, t_{PG}, t_{LMP*}^{(p)}\}$ and a proper-time family $\{t_{HF}^{(p)}, t_{PG}, t_{DF}^{(p)}\}$. The proper-time family intersects the GH family when $p = 2$, and intersects the LMP family for the case of $p = 1$ (PG time). In particular, the LMP and proper time families represent a successful familial classification of two distinct one-parameter generalizations of Painlevé-Gullstrand coordinates.

ACKNOWLEDGMENTS

The author gratefully acknowledges fruitful correspondence with Brandon DiNunno and Richard Matzner; commentary from Tristan Hubsch and Bernard Kelly; discussions with James Lindesay that introduced him to Painlevé-Gullstrand coordinates; support from the Howard University Department of Physics and Astronomy, where this work was begun; and support from a NASA Postdoctoral Fellowship through the Oak Ridge Associated Universities.

Appendix A: Lemaître coordinates: A time-dependent metric adapted to the rain frame

It is instructive to explore the matters of Sections II for a coordinate system which gives the Schwarzschild metric an explicit time dependence. This scheme begins by noting that the motion of an infalling $\tilde{E} = 1$ particle can be determined by solving (2.6), with the result being

that the trajectory $r[\tau]$ takes the form

$$r[\tau] = \left(\frac{3}{2} \sqrt{2m} (\tilde{\tau}_0 - \tau) \right)^{2/3}, \quad (\text{A1})$$

where $\tilde{\tau}_0$ is a constant, equal to the value of τ at which the particle reaches the black hole singularity. Physical quantities associated with these geodesics are used as coordinates in the Lemaître system [10], beginning with the proper time τ . However, as discussed in Section II, for an infalling $\tilde{E} = 1$ observer, $\Delta\tau = \Delta t_{PG}$. Therefore we can substitute $\tau_0 - t_{PG}$ for $\tilde{\tau}_0 - \tau$ in (A1), yielding

$$r[t_{PG}] = \left(\frac{3}{2} \sqrt{2m} (\tau_0 - t_{PG}) \right)^{2/3}. \quad (\text{A2})$$

The quantity τ_0 , the value of PG time at which a given particle reaches $r = 0$, can be used to label the geodesic for that particle. This τ_0 is then promoted to a coordinate “ ρ ” so that

$$r = r[t_{PG}, \rho] = \left(\frac{3}{2} \sqrt{2m} (\rho - t_{PG}) \right)^{2/3}, \quad (\text{A3})$$

$$dr = -\sqrt{2m/r} (dt_{PG} - d\rho). \quad (\text{A4})$$

Radially infalling $\tilde{E} = 1$ geodesics have constant values of ρ , and thus ρ plays the role of a comoving radial coordinate (that can take negative values). The Lemaître coordinates are $\{t_{PG}, \rho, \theta, \phi\}$, and curves of constant ρ (which delineate the infalling geodesics) are presented in Figure 10. When (A4) is substituted into the PG metric (2.2), the result is [12, 15]

$$ds^2 = -dt_{PG}^2 + \frac{2m}{r[t_{PG}, \rho]} d\rho^2 + r^2[t_{PG}, \rho] d\Omega^2, \quad (\text{A5})$$

where $r[t_{PG}, \rho]$ is given explicitly by (A3). The coordinate t_{PG} is always timelike, ρ is always spacelike, and there is no coordinate singularity at the horizon. Thus the Lemaître system provides a *diagonal* representation of the Schwarzschild geometry that is well-behaved everywhere outside the physical singularity at $r = 0$. However, this has come at the expense of giving the metric explicit time dependence.

Now, the volume within the black hole with respect to this slicing is the region along slices of constant t_{PG} between $r[t_{PG}, \rho] = 0$ and $r[t_{PG}, \rho] = 2m$. For this calculation the range of t_{PG} and ρ will be taken as $(-\infty, \infty)$, indicating that the first geodesics reached $r = 0$ at very large negative values of t_{PG} . We also have

$$\sqrt{{}^{(3)}g} = \sqrt{2m} r^{3/2} [t_{PG}, \rho] \sin\theta = 3m(\rho - t_{PG}) \sin\theta. \quad (\text{A6})$$

Hence we obtain

$$\begin{aligned} \text{Vol}_{Lemaître} &= \int_0^{2\pi} \int_0^\pi \int_{r[t_{PG}, \rho]=0}^{r[t_{PG}, \rho]=2m} \sqrt{{}^{(3)}g} d\rho d\theta d\phi \\ &= 4\pi \int_{r[t_{PG}, \rho]=0}^{r[t_{PG}, \rho]=2m} 3m(\rho - t_{PG}) d\rho. \quad (\text{A7}) \end{aligned}$$

It is pleasantly straightforward to see from (A3) that $r[t_{PG}, \rho] = 0$ corresponds to $\rho = t_{PG}$, and $r[t_{PG}, \rho] = 2m$ corresponds to $\rho = t_{PG} + 4m/3$; the latter relation is illustrated graphically in the bottom panel of Figure 10. Consequently,

$$\begin{aligned} \text{Vol}_{Lemaître} &= 12\pi m \int_{t_{PG}}^{t_{PG}+4m/3} (\rho - t_{PG}) d\rho \quad (\text{A8}) \\ &= 6\pi m (\rho^2 - 2\rho t_{PG}) \Big|_{\rho=t_{PG}}^{\rho=t_{PG}+4m/3} = \frac{32\pi}{3} m^3. \end{aligned}$$

The time dependence has been completely eliminated, leaving precisely the volume obtained in (2.8). Even though this result merely confirms what one would expect based on the results of Section II, it is still satisfying to see it arise from a computation with both a time-dependent integrand and time-dependent limits of the integral.

Appendix B: Relating gradients of time functions to four-velocity

Let u^a represent the four-velocity of an observer falling inward on a radial geodesic with energy per unit mass $\tilde{E} = 1/\sqrt{p}$. This motion satisfies, for any $p > 0$,

$$\frac{dr}{d\tau} = -\sqrt{\frac{1}{p} - \left(1 - \frac{2m}{r}\right)}. \quad (\text{B1})$$

In LMP-family coordinates (i.e. either t_{LMP} or t_{LMP*}), we have

$$u^a = \left(\sqrt{p}, -\sqrt{\frac{1}{p} - \left(1 - \frac{2m}{r}\right)}, 0, 0 \right), \quad (\text{B2})$$

$$u_a = \left(-\frac{1}{\sqrt{p}}, 0, 0, 0 \right). \quad (\text{B3})$$

In proper time-family coordinates (i.e. either t_{DF} or t_{HF}), we have

$$u^a = \left(1, -\sqrt{\frac{1}{p} - \left(1 - \frac{2m}{r}\right)}, 0, 0 \right), \quad (\text{B4})$$

$$u_a = (-1, 0, 0, 0). \quad (\text{B5})$$

In reference [5] it was shown for the $p < 1$ case that one can relate u_a to the gradient of a time function, in this case t_{LMP} :

$$u_a = -\frac{1}{\sqrt{p}} \partial_a t_{LMP}. \quad (\text{B6})$$

This is consistent with (B3), but more general, since it holds in any coordinate system.

Since $t_{HF} = t_{LMP}/\sqrt{p}$ we also have

$$u_a = -\partial_a t_{HF}. \quad (\text{B7})$$

If one considers instead an observer with $p > 1$, the same reasoning leads to

$$u_a = -\partial_a t_{DF}, \quad (\text{B8})$$

and since $t_{LMP*}^{(p)} = \sqrt{p} t_{DF}^{(p)}$ we are led to

$$u_a = -\frac{1}{\sqrt{p}} \partial_a t_{LMP*}. \quad (\text{B9})$$

Comparison of (B6) with (B9), and (B7) with (B8) illustrates how t_{LMP*} is the $p > 1$ analog of t_{LMP} , and t_{DF} is the $p > 1$ analog of t_{HF} .

-
- [1] Hartle, J. *Gravity: An Introduction to Einstein's Relativity*. Addison Wesley, San Francisco, (2003).
- [2] Misner, C., Thorne, K. and Wheeler, J. *Gravitation*. W.H. Freeman, New York, (1973).
- [3] Poisson, E. *A Relativist's Toolkit: The Mathematics of Black-Hole Mechanics*. Cambridge University Press, New York, pp.167-68, (2004).
- [4] Taylor, E. and Wheeler, J. A. *Exploring Black Holes: Introduction to General Relativity*. Addison Wesley Longman, San Francisco, pp. B4-B13, (2000).
- [5] Martel, K. and Poisson, E. "Regular Coordinate Systems for Schwarzschild and Other Spherical Spacetimes," *Am. J. Phys.* **69**, 476-480 (2001), arXiv:gr-qc/0001069.
- [6] Francis, M. and Kosowsky, A. "Geodesics in the Generalized Schwarzschild Solution," *Am. J. Phys.* **72**, 1204-1209 (2004), arXiv:gr-qc/0311038.
- [7] DiNunno, B. and Matzner, R. "The Volume Inside a Black Hole," *Gen. Rel. Grav.* **42**, 63-76 (2010), arXiv:0801.1734 [gr-qc].
- [8] Painlevé, P. and Hebd, C.R. "La mécanique classique et la théorie de la relativité," *Acad. Sci. Paris, C. R.* **173**, 677680 (1921).
- [9] Gullstrand, A. "Allgemeine Lösung des statischen Einkörperproblems in der Einsteinschen Gravitationstheorie," *Ark. Mat., Astron. Fys.* **16**, 115 (1922).
- [10] Lemaître, G. *Annales de la Société Scientifique de Bruxelles*, Ser. A., **53**, 51-85 (1933).
- [11] Lake, K. "A Class of Quasi-stationary Regular Line Elements for the Schwarzschild Geometry," (1994), arXiv:gr-qc/9407005.
- [12] Gautreau, R. and Hoffmann, B. "The Schwarzschild radial coordinate as a measure of proper distance," *Phys. Rev. D* **17**, 2552-2555 (1978).
- [13] Hamilton, A. and Lisle, J. "The River Model of Black Holes," *Am. J. Phys.* **76**, 519-532 (2008), arXiv:gr-qc/0411060.
- [14] Novikov, I. Doctoral dissertation. Shternberg Astronomical Institute, Moscow (1963).
- [15] Blau, M. "Lecture Notes on General Relativity," (2014), www.blau.itp.unibe.ch/GRlecturenotes.html.
- [16] Bini, D., Geralico, A. and Jantzen, R. "Separable Geodesic Action Slicing in Stationary Spacetimes," *Gen. Rel. Grav.* **44**, 603-621 (2012), arXiv:1408.5259 [gr-qc].
- [17] Parikh, M. and Wilczek, F. "Hawking Radiation as Tunneling," *Phys. Rev. Lett.* **85**, 5042-5045 (2000), arXiv:hep-th/9907001.
- [18] Adler, R., Bjorken, J., Chen, P. and Liu, J. "Simple Analytic Models of Gravitational Collapse," *Am. J. Phys.* **73**, 1148-1159 (2005), arXiv:gr-qc/0502040.
- [19] Poplawski, N. "Radial motion into an Einstein-Rosen bridge," *Phys. Lett. B* **687**, 110-113 (2010), arXiv:0902.1994 [gr-qc].
- [20] Gautreau, R. "Geodesic Coordinates in the de Sitter Universe," *Phys. Rev. D* **27**, 764-778 (1983).
- [21] Gautreau, R. "Imbedding a Schwarzschild mass into cosmology," *Phys. Rev. D* **29**, 198-206 (1984).
- [22] Posada, C. "Imbedding a Reissner-Nordström Charged Mass into Cosmology," arXiv:1405.6697 [gr-qc].

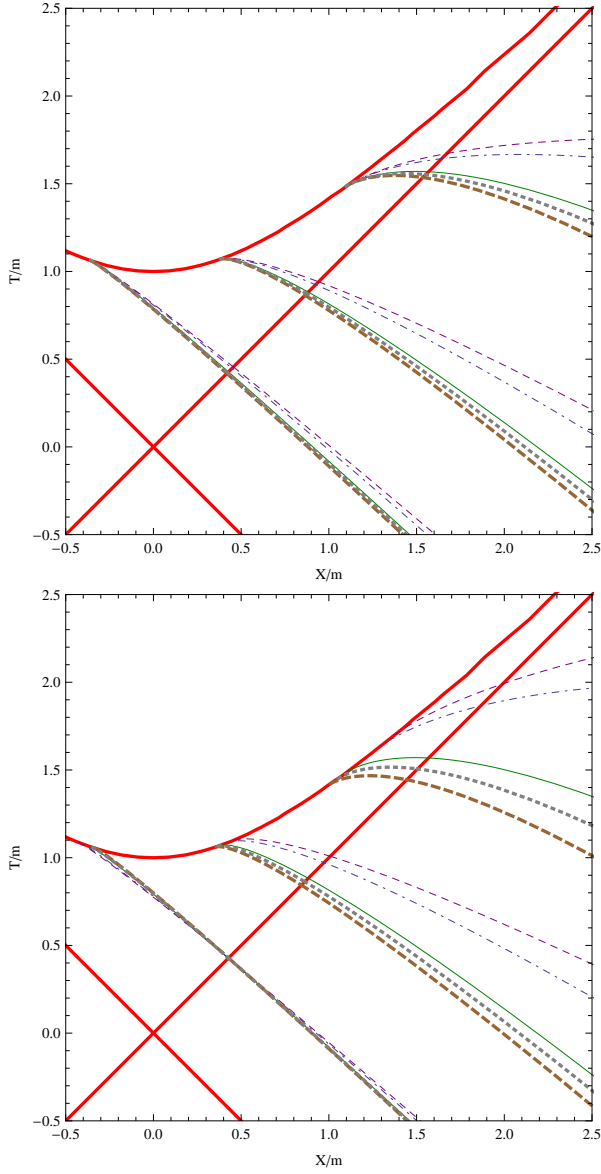


FIG. 9. Top panel: Plots from the LMP family, containing curves of constant t_{LMP} along with curves of constant t_{LMP^*} and constant t_{PG} . The lower bundle corresponds to $\{t_{LMP}, t_{PG}, t_{LMP^*}\} = -1.4m$; the middle and upper bundles to $1.5m$ and $3.8m$ respectively. Within each bundle, from the bottom, the values of p are $\{7/8, 15/16, 1, 9/7, 7/5\}$, and within any given bundle the curves do not cross. Bottom panel: Plots from the proper-time family. The lower bundle corresponds to $\{t_{HF}, t_{PG}, t_{DF}\} = -1.4m$; the middle and upper bundles to $1.5m$ and $3.8m$ respectively. Each bundle contains a range of p values given by, from the bottom, $\{7/8, 15/16, 1, 9/7, 7/5\}$. For the proper-time family, when a bundle corresponds to a negative value of time, its curves *do* cross, as can be seen in the lower bundle.

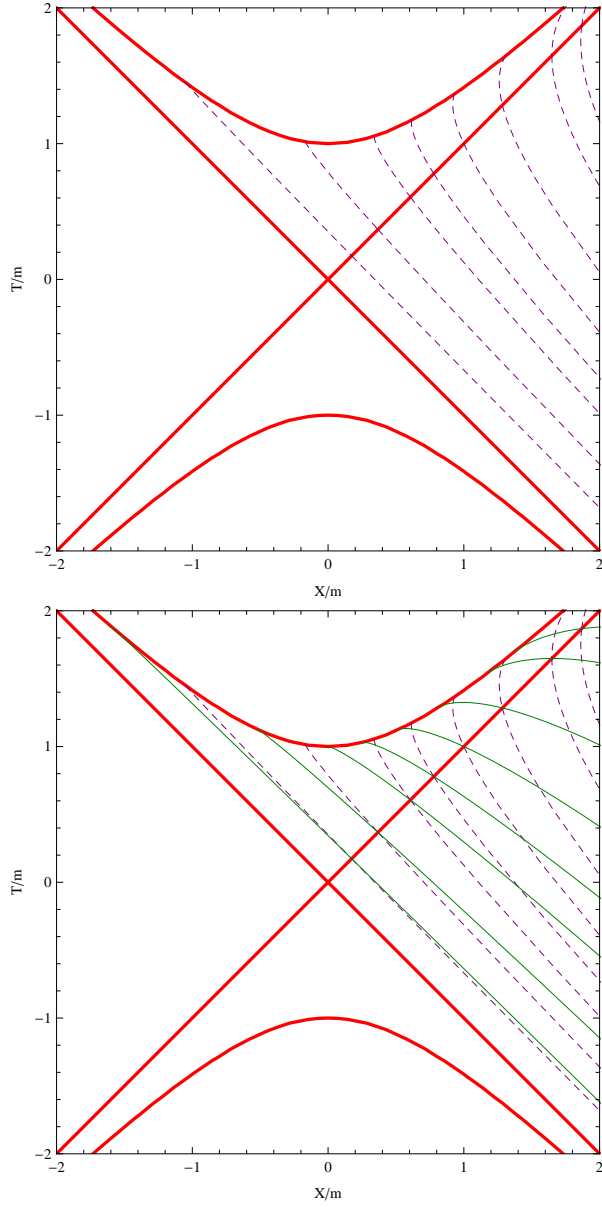


FIG. 10. Top panel: Dashed curves of constant ρ , i.e. infalling radial geodesics. From the left, these curves denote the cases $\rho = \{-11m/3, -2m/3, 4m/3, 7m/3, 10m/3, 13m/3, 16m/3, 35m/6\}$. Bottom panel: The same geodesics (dashed) from the top panel, now shown together with (thin solid) curves of constant t_{PG} . The curves of constant PG time, correspond to $t_{PG} = \{-5m, -2m, 0, m, 2m, 3m, 4m, 4.5m\}$. Each of these t_{PG} curves has a corresponding geodesic that intersects it precisely at $r = 2m$; such a geodesic satisfies $\rho = t_{PG} + 4m/3$.